

## Intrinsic Damage Assessment of Beam Structures Based On Structural Damage Indicators

Andreas Preisler<sup>1</sup>, Kai-Uwe Schröder<sup>1</sup>, Martin Schagerl<sup>2</sup>

<sup>1</sup>Institute of Structural Mechanics and Lightweight Design, RWTH Aachen University, Germany

<sup>2</sup>Institute of Constructional Lightweight Design, Christian Doppler Laboratory for Structural Strength and Control of Lightweight Constructions, Johannes Kepler University Linz, Austria

Corresponding Author: Andreas Preisler

**ABSTRACT:** One of the main challenges of current Structural Health Monitoring (SHM) systems is the trade-off between system complexity and system sensitivity. This contribution proposes to use structural analysis for an increase in sensitivity and efficiency. Comparing the structural behavior of the undamaged and damaged structure, optimized Structural Damage Indicators (SDI) are derived. Due to their zero-baseline, they enable an efficient monitoring based on a True or False statement. Structural models are used as digital baseline for an intrinsic damage assessment. This approach is shown in detail for beam structures, which are widespread in all fields engineering. In case of a bending dominated load case, strain at the neutral axis is proposed as SDI. For longitudinal forces, a zero-strain direction is derived as a purely material dependent parameter. Here, strain in zero-strain direction is used as SDI. The combination of both SDIs enables an efficient SHM for arbitrary loaded beam structures.

**KEYWORDS** Beam Structures, Damage Assessment, Damage Detection, Structural Damage Indicator, Structural Health Monitoring

Date of Submission: 19-05-2018

Date of acceptance: 04-06-2018

### I INTRODUCTION

Within the last decades, lightweight design has evolved to an advanced state. Starting from the general principles of lightweight design, the vast growth of computational power has made analysis of complex structures feasible. However, lightweight design still faces a formidable challenge in the uncertainties present in the design process. For example, operational loads need to be estimated for sizing [1]. Therefore, safety factors are introduced to ensure a conservative estimation. Despite the extensive testing effort, material properties are also uncertain. They vary along with the quality of manufacturing process. Therefore, A-values and B-values are derived, where a certain amount of specimens are expected to equal or exceed the given strength with 95% of confidence [2]. Fatigue behavior of materials is a special concern. The occurrence of damage initiation and propagation can only be estimated. Since potential damages of a structure are not always noticed in service, they have to be considered during sizing process as well as damage propagation. Dependent on design philosophy, load redistribution due to damage is considered (fail-safe) and regular inspections are scheduled (damage tolerance) [3-4]. As a result, the fail-safe approach leads to additional weight, while a damage tolerant design increases maintenance cost. All in all, uncertainties lead to a conservative sizing process, which overestimates loads while underestimating strength of the structure.

Structural Health Monitoring (SHM) is the automatic and on-line observation of structural integrity during service. It provides a tool to overcome uncertainties and to guarantee structural integrity along with a reduced amount of inspections, made possible by the information provided by the SHM system.

In general, SHM detects deviations, which are referring to the presence of damage. More sophisticated systems aim at localizing, qualifying and quantifying damages in order to provide enough information for damage evaluation. According to Rytter [5], monitoring methods can thus be classified into four different levels of complexity:

- **Level 1 (detection)** provides qualitative information that a damage is present in the structure.
- **Level 2 (localization)** determines the location of the damage.

- **Level 3 (assessment)** determines the size of the damage.
- **Level 4 (consequence)** evaluates the actual safety of the structure.

With increasing level of diagnosis, complexity rises. Level 4 corresponds to a sophisticated SHM system, which is capable of decision-making. The SHM system can determine whether the detected damage is critical or not, whether immediate shut-down is required or not. In case of a non-critical damage, an estimation of residual strength and of the remaining lifetime is possible. This information is necessary in order to schedule maintenance. In addition to the classification by Rytter, SHM systems can be classified by their scope:

- **Global SHM** covers the whole structure in order to monitor all possible damages including accidental and impact damages.
- **Local SHM** focuses the monitoring effort on highly stressed or safety-critical areas of the structure.

For global SHM systems, data-based (statistical) methods like pattern recognition [6] provide tools for detecting an abnormal behavior related to damages. However, those methods often struggle to cover more than the first two levels of complexity (detection and localization). Especially in case of local SHM systems, physical models can be used in order to link the structural behavior to the damage severity. These approaches are referred to as physical-based approaches. For example, Sigurdardottir [7] utilizes the shift of the neutral axis of bridges as a damage sensitive feature. The structural behavior is monitored with at least two fiber optical sensors within a cross-section, in order to determine the position of the neutral axis. Soman et al. [8] follow a comparable approach for wind turbines. The zero strain point for mixed load cases (bending and compression loads) is investigated.

This manuscript emphasizes the use of structural analysis as a foundation for local SHM systems. Based on the comparison of undamaged models with damaged models, efficient Structural Damage Indicators (SDI) are defined focusing on sensitivity. Previous work [9-10] presented this approach for purely bending loaded beams. Here, a new SDI for tension loaded truss elements based on zero-strain trajectories is derived. Combining both, the SDI for purely bending loaded beams and the new SDI for truss structures, arbitrary loaded beam structures can be monitored efficiently.

## II FUNDAMENTAL PRINCIPLES OF STRUCTURAL DAMAGE INDICATORS

The complete understanding of structural behavior is highly beneficial for setting up SHM systems. Primary and secondary load paths are understood, as well as highly stressed regions of the structure, potential damage mechanisms and their effect on the structural behavior. In general, damage is a local phenomenon. Although a more extensive damage might have a considerable effect on the global behavior of a structure (e.g. in terms of global stiffness reduction and change of global deformation), the majority of changes in structural behavior occurs in a local domain close to the damage (strain and stress redistribution). Therefore, an SHM system which focuses on a local domain is more sensitive than a system which monitors the global behavior.

If accidental damage (e.g. due to tool-drop or misused cases) has to be taken into account, a huge amount of combination of potential damage locations and damage types need to be considered. Thus, an enormous effort is needed in order to cover all combinations. This effort can be reduced if accidental damage is rare. In this case, it is sufficient to simply detect presence of the damage or of the accidental event itself and determine a rough location. This can be referred as a level 2 monitoring according to Rytter [5] and can be achieved by SHM systems which are focusing on global effects or using data-based methods (e.g. outlier detection). In case an accidental damage is detected, an inspection is triggered in order to assess the damage.

In reality, there is no perfect structure. Every structure has small inherent defects, e.g. pores or small flaws that do not have a measurable impact on the structural behavior. However, those defects are a potential source for damage initiation. Damage initiation and damage propagation may occur if those defects lie in highly stressed regions. Those kinds of damage are related to fatigue and their occurrence is very likely for optimized lightweight structures. However, such structures are analyzed in detail during sizing processes. Therefore, critical areas, so called hot spots [11], and the referring damage modes are already known. The monitoring effort is significantly reduced, if monitoring is focused on the hot spots.

This contribution proposes to use structural models not only for the sizing of a structure, but also for the design of SHM systems. The models used in sizing can also be used in order to determine the effect of the expected damage on the structural behavior. Comparing both, i.e. the structural behavior of the undamaged and the damaged structure, certain effects can be identified that refer to the presence of damage. Such effects provide very efficient damage indicators with a clear *True* or *False* statement. Due to their relation to the structural behavior, those damage indicators are referred to as structural damage indicators (SDI). A major advantage of those SDIs is that they are sensitive to all kind of damage which have an influence on the load carrying behavior. In addition, damage size and SDI are directly related. Therefore, the presence of a deviation indicates damage, while the amplitude of deviation corresponds to the severity of damage. Based on structural

analysis certain predefined thresholds corresponding to certain damage sizes can be defined in order to enable an intrinsic damage assessment. This represents a digital baseline.

In most cases, the damage indicator is defined as absolute deviation of a structural parameter  $X$  at position  $x$  from its expected value:

$$t_{abs} = X(x, t) - X_0(x) \tag{1}$$

$X_0(x)$  describes the expected measurement (reference value, baseline), and  $X(x, t)$  the actual measurement of the structure at time  $t$ . However, the absolute damage indicator does not provide an information about sensitivity of the measurement. If the reference value is rather high, the change in signal might be lost in the measurement noise. Thus, a relative damage indicator [10] is considered:

$$t_{rel} = \frac{X(x, t) - X_0(x)}{X_0(x)} \tag{2}$$

Eq. (2) demonstrates that a reference value  $X_0(x)$  of zero or close to zero is very beneficial. In this case, a rather weak signal, which means a small change of the measurement value  $X(x, t)$ , leads to a strongly amplified change of the damage indicator  $t_{rel}$ . In case of an undamaged structure, the damage indicator is zero and no data needs to be sent, processed or stored.

In summary, this contribution follows two principle ideas:

- **Structural analysis** is used in order to predict the influence of the damage on the structural behavior. Instead of measuring the damage itself by using measurements close to the damage, optimized SDIs are considered based on a zero baseline. This provides a clear *True* or *False* statement.
- The knowledge coming from the structural analysis is the foundation for a **digital baseline**. Based on the analysis certain threshold values are defined. This approach enables an efficient intrinsic damage assessment.

As a result, this approach shifts the effort from complex monitoring systems to more detailed preliminary analyses before setting up the actual SHM system. In this respect, synergies between the sizing process and the design of the SHM system can be exploited.

### III STRUCTURAL DAMAGE INDICATORS FOR BENDING BEAMS

Many structures are idealized as beams. Beams are structural elements which extend mainly in longitudinal direction (length  $\gg$  (width, height)) and which are mainly subjected to bending. This section neglects all other section forces. They will be considered separately in later sections and then superimposed.

Considering linear elastic material behavior, longitudinal stresses in a straight beam are linearly distributed as shown in Fig. 1 (left). For pure bending, the stress becomes zero at the cross-section's centroid. The line which is connecting all centroids, is therefore referred to as neutral axis. Longitudinal stresses under the bending moment  $M_2$  depend on the distance  $x_3$  to the centroid and on the cross-section's second moment of inertia  $J_{22}$ :

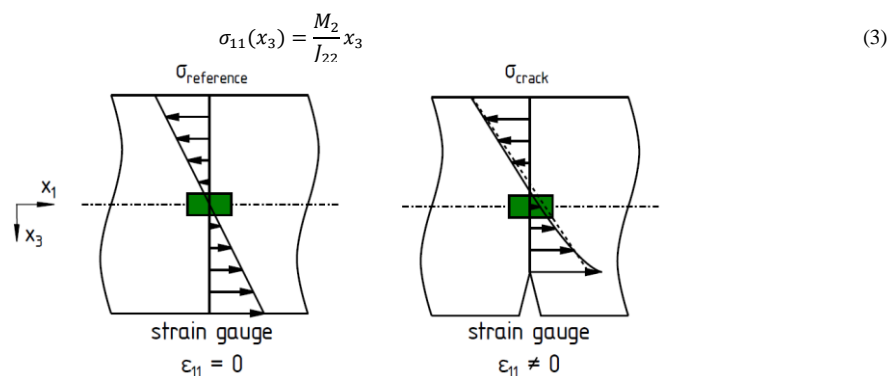


**Fig. 1: Distribution of longitudinal stress for an undamaged (left) and a cracked (right) beam element [9]**

In case of beam structures, cracks at the tension-loaded edges are a potential source of failure. If a crack is present, the cracked area is not able to transfer any load. This results in modified properties of the cross-section. As sketched in Fig. 2 for a thin-walled rectangular profile, the effective centroid is shifted and thus the origin of the coordinate system is shifted by an amount of  $\Delta x_3$ . Due to the loss of profile's height, the cross-section's moment of inertia is reduced as well. Overall, stress is redistributed, the neutral axis is shifted and the stress gradient is increased.

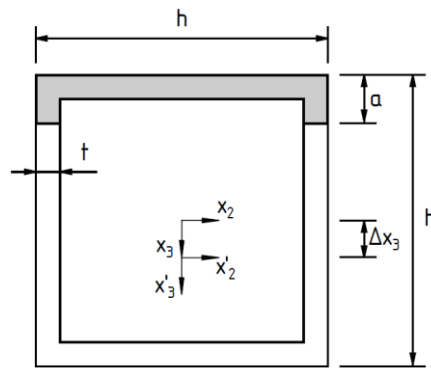


**Fig. 2: Shift of the effective centroid due to crack (marked by the grey area) and definition of  $h$ ,  $t$ ,  $a$  and  $\Delta x_3$**

The effective cross-sectional properties can be estimated by simply disregarding the damaged area. For a crack that effects symmetrically the whole width of the profile, the influence of the crack length on the position of the effective centroid and on cross-section's second moment of inertia are plotted in Fig. 3 for a ratio of height to thickness  $h/t = 20$ . As a remark, from fatigue analysis point of view this is a rather artificial case. Already for rather small crack lengths ( $a < t$ ), the second moment of inertia is reduced drastically. When the crack length reaches cross-sections thickness  $t$ , the upper flange is separated completely. At this point, the effective second moment of inertia is approximately 50% of the initial value. Afterwards, the slope of the curve is reduced. The influence of a crack growth within the web on the second moment of inertia is less severe. A comparable trend is observed for the shift of centroid. For small crack lengths ( $a < t$ ), the effective centroid is changing quickly to a value of approximately 18% of cross-sections height. After the upper flange is completely separated, a smaller slope is present. In case of cracks in both flanges, compressive stresses lead to crack closure at one flange. Thus, the direction of the shift is dependent on the algebraic sign of the bending moment. However, this analytical estimation assumes linear stress distribution. Stress concentration (respectively stress intensity) at the crack tip is neglected. It shall be noted, that stress concentration reduces the previously mentioned effect, as sketched in Fig. 1 (right).

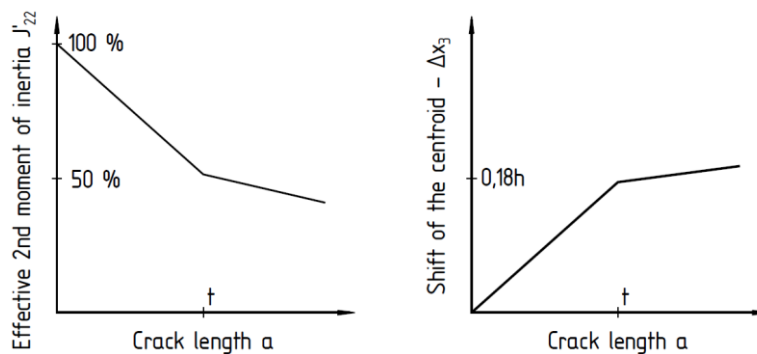


**Fig. 3: Analytical calculation of cross-sections effective moment of inertia (left) and change of the effective centroid (right) due to crack for a ratio of  $h/t = 20$  (see Fig. 2)**

Based on the fundamental principles of the structural damage indicators, the authors propose to measure strain at the neutral axis, rather than monitor the position of the neutral axis based on distributed strain sensors. In case of the undamaged structure, a load independent zero-strain signal is obtained. If a damage is present, a clear deviation from zero is measured and therefore the damage is detected. High sensitivity is indicated by Eq. (2). The amount of strain deviation then is dependent from load level, from severity of the damage and the distance to the damage [9-10].

### 3.1 Test Setup

In order to verify the monitoring approach, measuring strain at the neutral axis as damage indicator, four point bending tests are performed. The test was already described in previous work [9]. However, its setup and results are summarized here in order to provide a comprehensive picture. The general test set-up of four point bending tests are shown in Fig. 4. The main area of interest is located between both load application

points. Within this segment, the bending moment has a constant maximum value, while all other section forces are zero. This leads to compressive stresses in the upper part of the cross-section. For thin-walled structures, stability problems are a potential failure mode in this area. The lower part is loaded by tension, where crack initiation might be the main source of failure. The presented study focuses on monitoring of potential cracks, as they can be detected in an early non-critical stage.

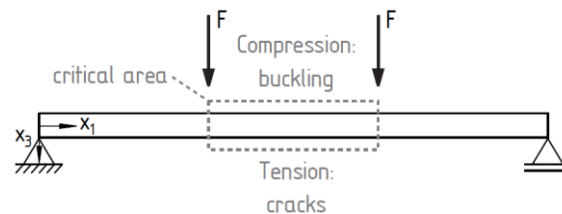


**Fig. 4: General test set-up for four point bending tests [10]**

For the four point bending tests, an aluminum tube with a rectangular cross-section is used. As indicated in Fig. 5, the damage is located in the symmetry plane and is artificially introduced by a saw cut which is gradually enlarged (1.0 mm, 2.5 mm, 4.0 mm and 5.0 mm). For each test, a maximum transverse force of  $F = 2$  kN is applied. The load application is realized with a servo-hydraulic cylinder pressing at the upper flange. The test setup is shown in Fig. 6

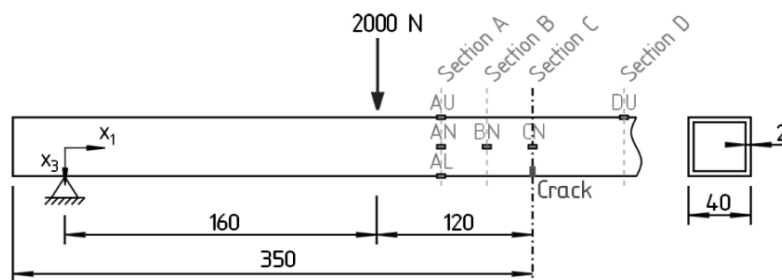


**Fig. 5: Geometry of test specimen and strain gages**



**Fig. 6: Test rig for the four point bending test**

In total, six strain gages are used during testing. The locations are shown in Fig. 5. The distance between the sections A, B and C is equal to the length of the cross-section's height (40 mm). Section C is the middle (symmetry) plane of the beam and hence the damaged cross-section. About this plane, sections D and A are symmetrically located. Strain gages AU and DU are located in the center of the upper, compressively loaded flange. Strain gage AL is located in the center of the lower, tension loaded flange. Strain gages AU, AL and DU are used for loads monitoring. For damage detection, strain gages AN, BN and CN are placed on the nominal center axis, i.e. at the neutral axis of the undamaged beam.

3.2 Test Results

Fig. 7 (left) shows strain gauge data for a crack length  $a = 2.5$  mm for all load steps. Strain gauges AU and DU show similar behavior, which indicates a proper symmetric loading of the specimen. In section A, almost pure bending behavior is present as both, strain gauge AU and strain gauge AL, are extended to almost the same absolute value of strain. Strain gauge AN shows a small amount of tensile strain. However, this strain value is negligible compared to strain gauges BN and CN. Strain gauges BN and CN are affected by the damage and show a distinct deviation from zero-strain. For higher loads, strain gauge CN shows a non-linear relationship between strain and load. This indicates a higher amount of plasticity at the crack tip due to stress concentration.

In order to reduce the effect of plasticity, further results are evaluated at a transverse force of 1 kN. The strain gauge data for BN and CN for varying crack lengths is evaluated in Fig. 7 (right). For small crack lengths ( $a = 1.0$  mm), compressive strain is present at the former neutral axis in the damaged cross-section. Although the influence of the shift of the effective centroid is small, the compressive value might be somewhat surprising. The answer lies in the stresses concentration near the crack tip. Due to their high leverage, they carry a noticeable amount of the tensile part of the bending moment. Thus, the global stress distribution is slightly shifted into the compressive regime. However, for a crack length  $a > 2.0$  mm, rather high tensile strains occur at the former neutral axis. In this case, the lower flange is completely separated and therefore the shift of cross-sections centroid is predominant.

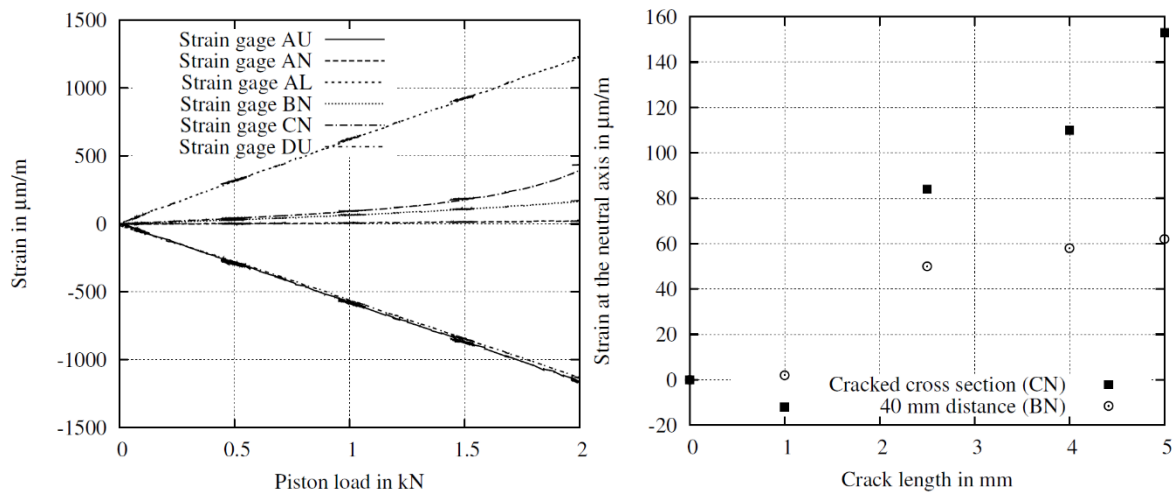


Fig. 7: Strain gauge data for a crack length of  $a = 2.5$  mm (left) and strain at BN and CN for varying crack lengths at transverse forces of 1 kN (right) [9]

3.3 Numerical Models

The numerical model was already described in previous works [9-10]. However, this article contains a more comprehensive evaluation of the results. The test is simulated combining two different modeling approaches using the commercially available tool ABAQUS 6.13-4. The major part of the specimen is modeled using shell elements. In close proximity to the crack, solid elements with incompatible modes are used in order to reproduce stress peaks at the crack tip and a flange, which might be only half-separated. Height and length of the refined area are set to  $0.75h = 30$  mm. Therefore, the area around the neutral axis close to the crack is also modeled with solid elements. In case of the shell elements, an average element length of  $h/20 = 2$  mm is considered. The average element length in case of solid elements is  $t/4 = 0.5$  mm. However, for crack lengths  $t/2 < a < t$ , a more refined mesh is considered, to ensure that there are at least two elements with intact connectivity over thickness direction within the damaged flange. In addition, the symmetry plane in the middle of the beam is used. The crack is within this symmetry plane. A sketch of the model is shown in Fig. 8.

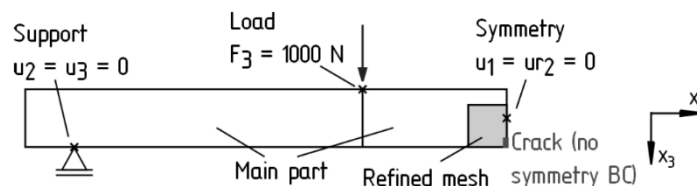


Fig. 8: Boundary conditions and meshing approaches of the FEM model [9]

The two different meshing approaches are joined with a tie constraint. The thickness of shell elements and their rotational degrees of freedom are considered. Boundary conditions are set in order to match the test setup shown in Fig. 6. Kinematic couplings connect the vertical displacements of the upper side of the cross-section to the load application points to ensure proper loading. An additional kinematic coupling transfers the boundary condition to the lower side of the cross-section. Symmetry constraints are applied to all nodes lying on the symmetry plane except for nodes within the cracked area. This approach is comparable to introducing a crack by node separation. The test is modeled with a linear elastic, linear plastic material behavior with hardening. By that means, non-linear material behavior is described by linear approximation between yield strength and ultimate strength. The material data is summarized in Table 1. True stresses and strains are considered within the model.

**Table 1: Material data for Aluminium 2024-T3 (extrusion) [4]**

| Linear material data              |                            |
|-----------------------------------|----------------------------|
| $E$ – Young's modulus             | 74500 MPa                  |
| $\nu$ – Poisson's ratio           | 0.33                       |
| Non-linear material data          |                            |
| $R_{p0.2}$ – Yield strength       | 290 MPa                    |
| $R_m$ – Ultimate tensile strength | 395 MPa                    |
| $A_5$ – Ultimate tensile strain   | 12%                        |
| $K_{IC}$ – Fracture toughness     | 830 MPa $\sqrt{\text{mm}}$ |

### 3.4 Results of the Numerical Study

In order to verify the numerical results, the longitudinal strain is evaluated at strain gage positions. In Fig. 9, these values are compared with strain gage data obtained from tests. The numerical results show a perfect symmetry between the tension and compression loaded flanges, which refers to pure bending. Small deviations in the test data, are considered negligible.

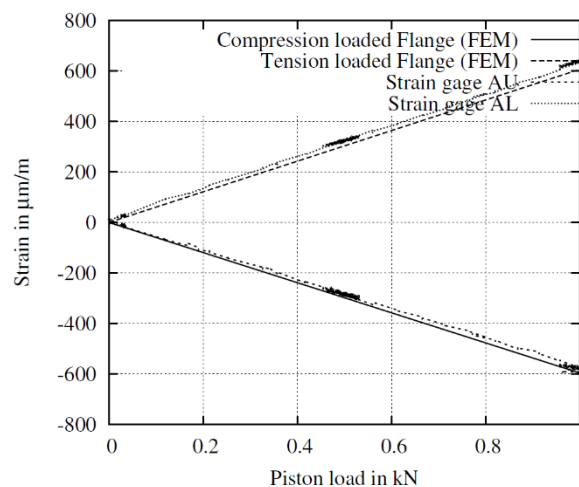


**Fig. 9: FEM flange strain compared to test data [9]**

The distribution of longitudinal strain in case of a crack  $a = 2$  mm, i.e. when the flange is just completely separated, is plotted in Fig. 10. For illustration, the deformation is scaled with a factor of 50 and the model is mirrored at its symmetry plane. Due to the crack, the tension-loaded flange is not able to carry any loads within the cracked cross-section. Stress redistribution occurs as well as stress peaks close to the crack tip. The curved crack front is caused by the shear lag effect.

Fig. 11 shows the relative change of strain as damage indicator  $\iota_{rel}$  (see Eq. (2)). The area marked grey refers to a change in signal below 100%. Red indicates sensor positions, where the signal is changed by at least 300%. In close vicinity to the crack tip, high changes in strain are present due to stress concentration. However, this value is rapidly decreasing. The relative change in strain is also very high in close proximity to the centerline and tends to infinity at the former neutral axis, due to a reference value, which is close to (or even equal) zero. Therefore, high values are achieved within a certain distance. This is in accordance to Saint-Venant's principle [12]. According to Saint-Venant's principle, disturbances fade away in a distance of the size of the cross-sections height  $h$ . Within this region, strain sensors will achieve high sensitivity.

The distribution of strain at the former neutral axis is plotted in Fig. 12 (left) over the distance to the cracked cross-section for multiple crack lengths. All cases show significant non-zero strain values within a distance of at least  $h = 40$  mm. The curves have a local minimum at the damaged cross-section. The maximum, which is reached at a distance of 15 to 20 mm, indicates that the effect of stress concentration decays fast. Although all curves show a comparable behavior, the magnitude is dependent on crack length. Especially in the case of a crack length  $a > 2$  mm, which represents a completely separated flange, high strains are present.

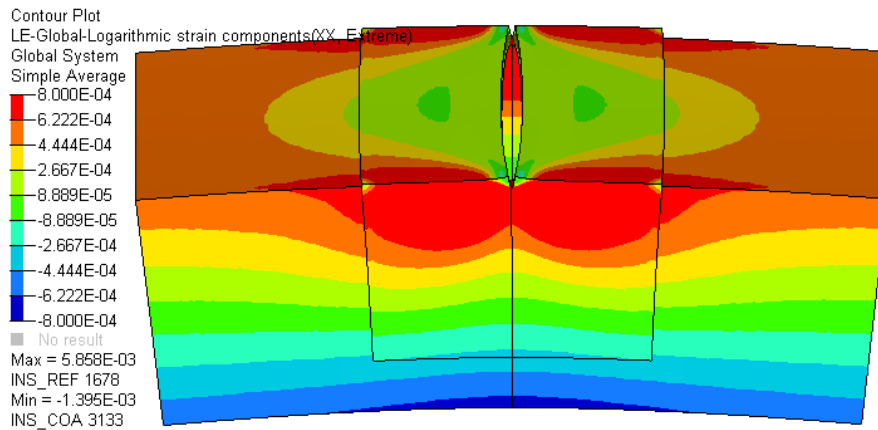


Fig. 10: Strain distribution in close distance to the crack for  $a = 2$  mm

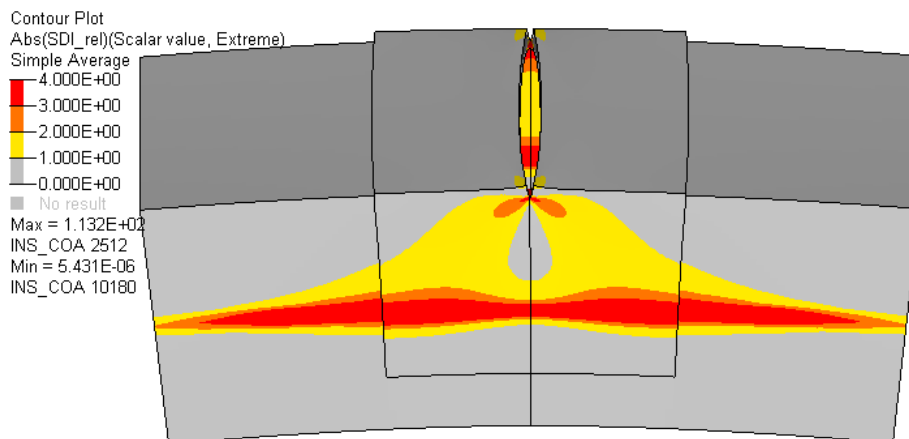


Fig. 11: Relative change of strain (see Eq. (2)) for  $a = 2$  mm

It is very important to determine whether a crack can be detected before it reaches a critical size. Therefore, a definition of a critical crack size is needed. For example, according to regulations of aeronautical engineering [3-4], structures are sized with a safety factor of 1.5 with respect to the expected load level; the so-called design load. Within the expected load level, no detrimental permanent deformation is allowed. However, if a damage is present, the residual strength has to be at least larger than the design load (i.e. without considering the safety factor). Thus, a crack is considered as critical, if residual strength falls below the design load.

The numerical analysis shows that final failure of the undamaged beam occurs at a transverse force level of  $F_{ult} = 7662$  N. Therefore, the maximum possible design load is derived from the ultimate strength value by considering the reciprocal of the factor 1.5:

$$F_d = \frac{1}{1.5} F_{ult} = 5108 \text{ N} \tag{4}$$

This load level is also below the onset of plasticity for an undamaged beam. As required, permanent deformation does not appear.

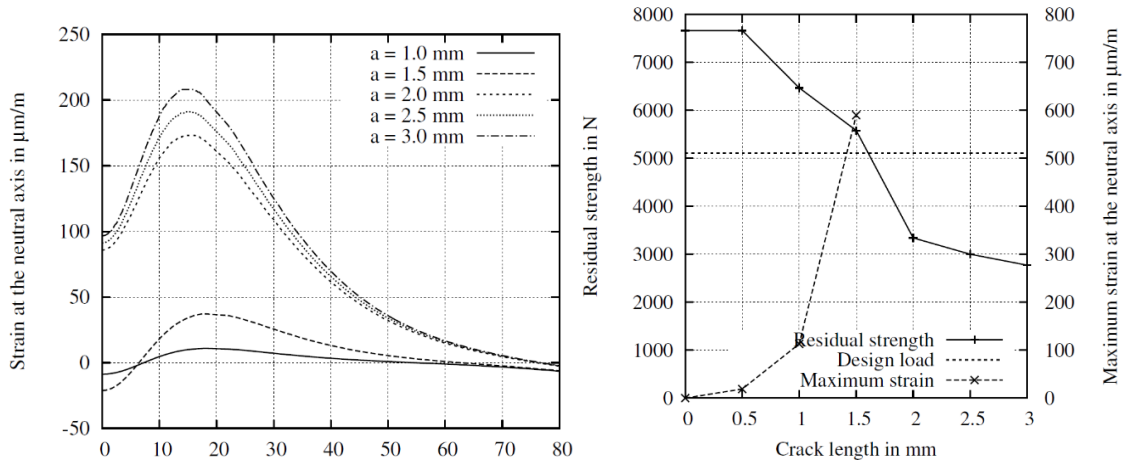


**Fig. 12: Influence of the distance to the crack on the strain at the former neutral axis [9] (left) and residual strength and maximum deviation of strain due to crack (right)**

The residual strength for a varying crack length is plotted in Fig. 12 (right). An increasing size of the crack leads to a reduced effective cross-section and to more severe stress concentration. Therefore, the residual strength is reduced. The most significant loss of residual strength takes place until the complete separation of the flange ( $a = 2$  mm). After separation of the flange, an increasing crack length has less influence. However, in this case, the residual strength is below than the design load and a critical crack is present. According to Fig. 12 (right) the crack becomes critical if  $a > 1.6$  mm.

In addition to the residual strength, Fig. 12 (right) shows the maximum value of strain along the neutral axis at design load. In case of a very small crack ( $a = 0.5$  mm), the maximum strain is  $19 \mu\text{m}/\text{mm}$ . However, the influence of such a crack on the residual strength is negligible. For larger cracks, the maximum amount of strain on the former neutral axis is increasing exponentially. A crack of  $a = 1.0$  mm can be easily detected, due to a maximum amount of strain of  $113 \mu\text{m}/\text{mm}$ . Therefore, we conclude that cracks in beams can be reliably detected in the pre-critical stage if strain at the nominal neutral axis is monitored.

#### IV STRUCTURAL DAMAGE INDICATORS FOR TRUSS ELEMENT

Truss elements are structural elements, which extend are mainly in longitudinal direction (length  $\gg$  (width, height)) and which are mainly exposed to longitudinal forces. If longitudinal forces act exactly at the neutral axis, longitudinal strain is evenly distributed over the whole cross-section. If a crack occurs, two main effects are present: (1) Due to the shift of the centroid, minor bending is present in the damaged cross-section leading to a linear strain distribution. (2) Stress concentration arises at the crack tip. However, using those effects for damage detection is not efficient, due to the high reference value of longitudinal strain.

Very promising SDIs can be derived by applying the approach introduced by Schagerl et al. [13] to truss structures. For damage detection on surfaces which are subjected to a two-dimensional strain state, Schagerl et al. derive so-called zero-strain trajectories. Along these trajectories, the strain is ideally zero and has thus optimal reference value. The idea is illustrated with Mohr's circle in Fig. 13. In case of a truss element and a coordinate system, whose  $x_1$ -axis coincides with the longitudinal direction of the truss, the in-plane strain state is described by the strains, where  $N_1$  denotes the longitudinal force and  $EA$  denotes the extensional stiffness:

$$\epsilon_{11} = \frac{N_1}{EA} \tag{5}$$

$$\epsilon_{33} = -\nu \frac{N_1}{EA} \tag{6}$$

$$\epsilon_{13} = 0 \tag{7}$$

If the coordinate system is rotated in-plane by  $\beta$ , the component of longitudinal strain  $\epsilon_{nn}$  changes according to:

$$\epsilon_{nn} = \frac{\epsilon_{11} + \epsilon_{33}}{2} + \frac{\epsilon_{11} - \epsilon_{33}}{2} \cos(2\beta) + \epsilon_{13} \sin(2\beta) \tag{8}$$

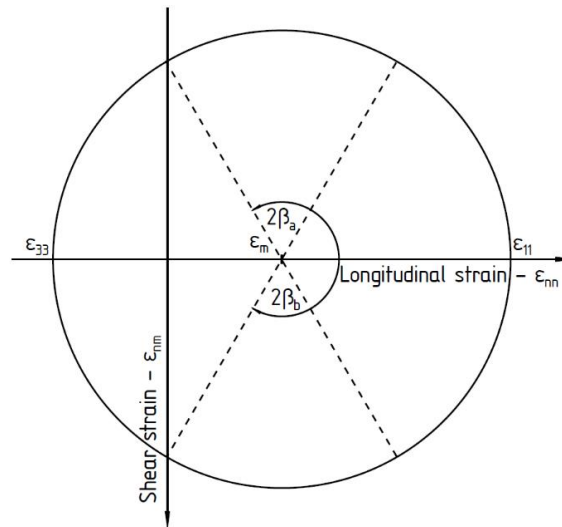


Fig. 13: Mohr's circle for truss-like structures

As indicated by Eq. (2), sensitivity is optimized, if the reference value is zero. This indicates  $\epsilon_{nm} = 0$ , in order to use longitudinal strain as a most efficient SDI. In case of a truss element where  $\epsilon_{33} = -\nu\epsilon_{11}$  and  $\epsilon_{13} = 0$ , the corresponding angles  $\beta_{a,b}$  are derived as:

$$\beta_{a,b} = \pm \frac{1}{2} \arccos\left(\frac{\nu - 1}{\nu + 1}\right) \tag{9}$$

These values are referred as zero-strain directions. For truss structures, zero-strain directions are independent from the amount of load and from the shape of the cross-section. They only depend on Poisson's ratio. As in all other linear problems with a single specific load-case, zero-strain directions are a material property. Due to this fact, it is very promising to search for zero-strain directions for monitoring. If a crack occurs, stress is redistributed. As a consequence, longitudinal strains  $\epsilon_{11}$  and  $\epsilon_{33}$  change and a considerable amount of shear strain  $\epsilon_{13}$  might appear, which contradicts the assumptions made for deriving the zero-strain directions. Longitudinal strain measured in these directions will be non-zero in case of a crack.

Positive and negative solutions, as sketched in Fig. 13, can be considered. Both directions are sensitive to damage. However, in one direction shear strain is positive, while in the other shear strain is negative. Therefore, both directions yield different amounts of strain in case of a damage. Fig. 14 emphasizes this fact by showing the trajectories of principle stresses. Shear strain due to damage is point-symmetric, while change of longitudinal strain is axisymmetric. As a result, both damage indicators are not symmetric to the crack plane.

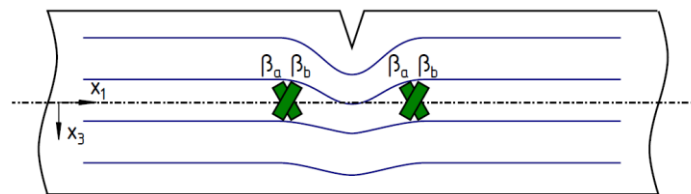


Fig. 14: Deviation of principle strain trajectories due to a crack

#### 4.1 Numerical Models

In this section, numerical models for analyzing truss structures are created based on previous models for bending beams (see Fig. 8 and Table 1). Geometry, meshing techniques and element size are maintained. However, boundary conditions are slightly changed. Reference in the cross-section's centroid are connected to the whole cross-section via kinematic couplings. The normal force is applied at reference point of the sliding support with the amount of 13260 N. By that means, maximum stresses of the undamaged beam and the undamaged truss are equal. The resulting model is sketched in Fig. 15.

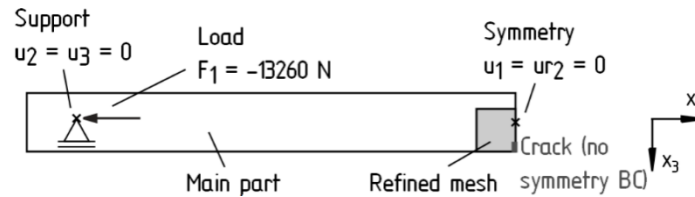


Fig. 15: Boundary conditions and meshing approaches FEM model for truss-like structures

4.2 Results of the Numerical Study

The distribution of longitudinal strain in case of a crack  $a = 2$  mm is plotted in Fig. 16. For illustration, the deformation is scaled with a factor of 50 and the model is mirrored at its symmetry plane. Longitudinal stresses are redistributed due to presence of crack leading to stress and strain peaks close to the tip of the crack. The height of strain peaks depends on the severity of the damage and on the load level. In case of a completely separated flange ( $a \geq 2$  mm), the damage is considerably severe and stress redistribution consequently large.

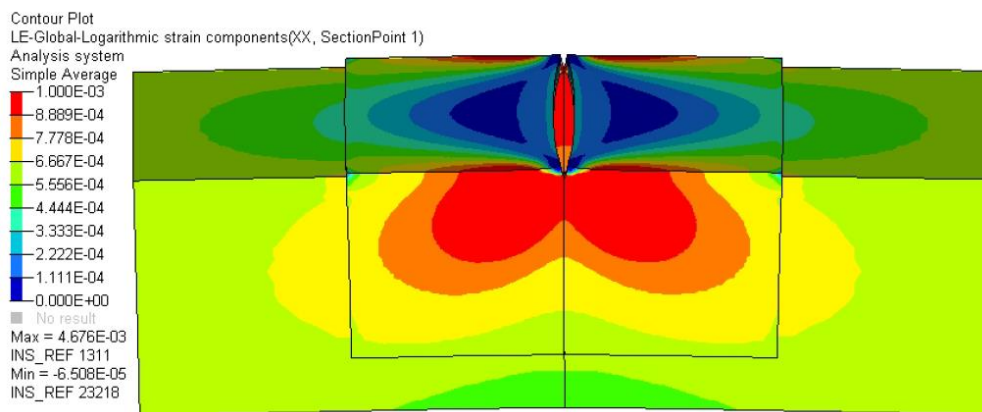


Fig. 16: Strain distribution in close distance to the crack for  $a = 2$  mm

The distribution of longitudinal strain and shear strain at the centroids of the cross-section for a crack length of  $a = 2$  mm is plotted in Fig. 17. Noticeable deviations occur close to the crack. For higher distances ( $x_1 > 80$  mm), the normal strains and the shear strain converge to their reference values (see Eqs. (5-7)). Measuring the longitudinal strain  $\epsilon_{11}$  or the transversal strain  $\epsilon_{33}$  for damage detection is actually not optimal as their reference value is not zero. Using shear strain  $\epsilon_{13}$  for damage detection may also be avoided, as its measurement requires strain gauge rosettes.

For the chosen material (see Table 1), zero-strain directions are rotated by  $\beta_{a,b} = \pm 60.12^\circ$  with respect to the  $x_1$ -axis (see Eq. (9)). The strains in these directions are monitored at the centroid of the cross-section. With that choice, cracks at both flanges can be studied with same sensitivity at one single measuring location. The change of strain in the former zero-strain direction due to crack is plotted in Fig. 18 (left) for the positive direction angle and in Fig. 18 (right) for the negative one. For a crack  $a < 2$  mm that refers to a flange, which is partly intact, the change of strain is almost zero at the cracked cross-section. The change of normal strain due to stress extrema is negligible (shear is actually not present in the cracked cross-section). For larger cracks, the change of normal strain is not negligible. The strain within the cracked cross-section is non-zero and the strain extrema are shifted. The comparison between the positive and negative directions yields that the negative shows a higher absolute value of strain. However, the positive direction leads to a higher sensitivity for larger distances from the cracked cross-section.

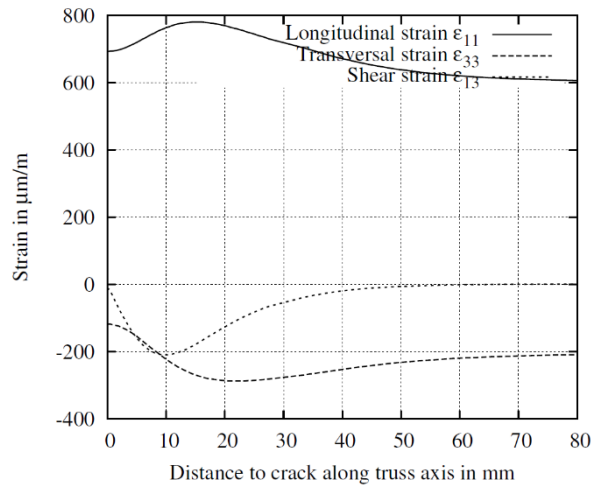


Fig. 17: Distribution of normal strain and shear strain at the position of the centroid

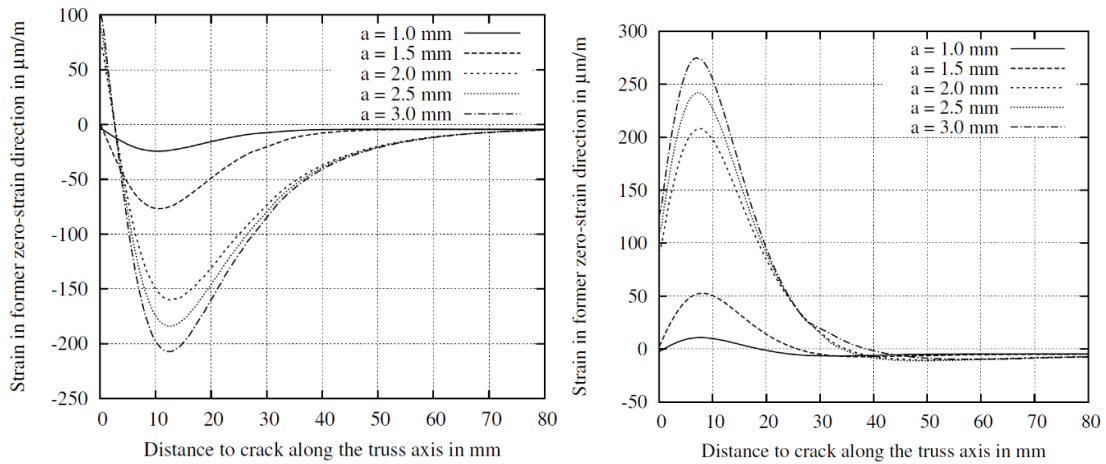


Fig. 18: Strain due to damage in the former zero-strain direction  $\beta_a = +60.12^\circ$  (left) and  $\beta_a = +60.12^\circ$  (right)

In order to assess the sensitivity of the introduced SDI, a critical crack length is derived according to regulations [3-4]. Numerical analysis shows that final failure of the undamaged truss occurs at a longitudinal force of  $F_{ult} = 88190$  N. The maximum possible design load is derived from the ultimate strength value by considering a safety factor of 1.5:

$$F_d = \frac{1}{1.5} F_{ult} = 58793 \text{ N} \tag{10}$$

This load level is also below the onset of plasticity. Therefore, permanent deformation will not occur as well. Residual strength of the cracked truss is plotted in Fig. 19 versus the crack length. The results are very similar to the results for beams. The most significant loss of residual strength takes place until the complete separation of the flange ( $a = 2$  mm). However, residual strength falls below design load in case of a crack length of  $a > 1.6$  mm. In addition, Fig. 19 shows the maximum value of strain due to a crack after applying design load. In case of a crack length of  $a = 1.0$  mm, the crack can be easily detected due to a maximum deviation of strain of  $126 \mu\text{m}/\text{mm}$ . Therefore, it is concluded that cracks in truss elements are reliably detected in pre-critical stages, if the strain in nominal zero-strain directions is monitored.

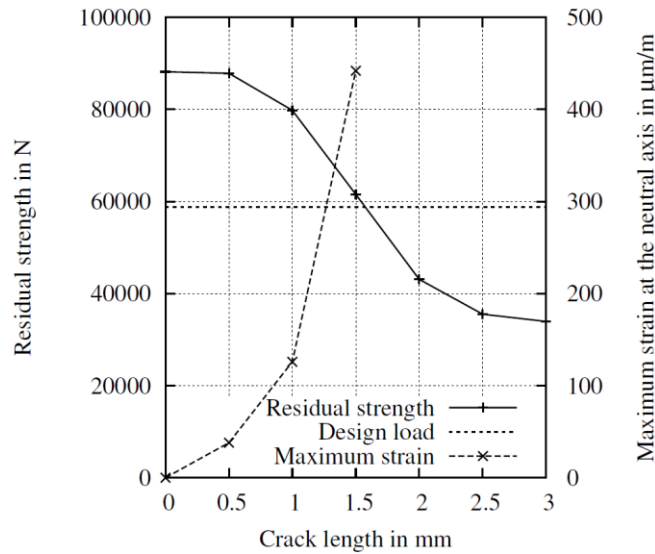


Fig. 19: Residual strength and maximum deviation of strain due to crack

V FURTHER CONSIDERATIONS FOR ARBITRARY BEAM STRUCTURES

Although many structures can be idealized as beams, pure bending or pure tension is rare. Often load cases are interacting. In these cases, at least a rough loads monitoring is crucial in order to distinguish different loads. In general, every loading can be divided up into six different cross-sectional forces and moments:

- Longitudinal force:  $N_1$
- Transverse forces:  $Q_2$  and  $Q_3$
- Torsional moment:  $M_1$
- Bending moments:  $M_2$  and  $M_3$

In the present article, torsional loading is not considered. Monitoring strain at the nominal neutral axis can be used for damage monitoring in case of an applied bending moment. Since only longitudinal strain  $\epsilon_{11}$  is monitored, shear strain due to transverse force or due to torsion is not relevant. However, longitudinal strain due to an additional longitudinal force *does* have an impact on this damage indicator.

If strain in a zero-strain direction is monitored, damage can be detected in case of a longitudinal force. This monitoring approach can be easily adapted if additional bending is present. However, the presence of additional shear strains (e.g. due to transverse forces) changes the zero-strain directions.

Active transverse forces over a certain distance cause bending moments. Thus, such load cases are accessible by monitoring the neutral axis. If a normal force is expected in addition to a bending moment, monitoring the neutral axis is still advantageous. In this case, the amplitude of the longitudinal force  $N_1$  is determined via loads monitoring. Using Eq. (5), the longitudinal strain at the neutral axis due to the normal force can then be subtracted from the sensor signal yielding the relative damage indicator:

$$t_{rel} = \frac{\left[ \epsilon_{11}(x_1, t) - \frac{N_1}{EA} \right] - \left[ \epsilon_{11,0}(x_1) - \frac{N_1}{EA} \right]}{\epsilon_{11,0}(x_1) - \frac{N_1}{EA}}$$

$$t_{rel} = \frac{\epsilon_{11}(x_1, t) - \epsilon_{11,0}(x_1)}{\epsilon_{11,0}(x_1) - \frac{N_1}{EA}} \tag{11}$$

In the case of both, absolute and relative damage indicators, the measured strain depends on two effects: (1) size of the crack (severity of the damage) and (2) distance to the damaged cross-section (location of the damage). In the case of the absolute damage indicator, the measured strain depends also on the load level. Even if loads monitoring is used in order to consider the effect of the load level, a single measuring point is not sufficient in order to distinguish between a small crack in close distance and a severe crack in far distance. Therefore, within the region of potential damages, at least two measuring points P1 and P2 with known distance  $\Delta x_1$  to each other are needed. In this case, the data can be evaluated by a simple set of curves [9-10]. Each curve refers to one specific crack length  $a$ . Then, simple algorithms can be used, which perform a loop over the distance of the sensors and afterwards a second loop over all curves. In order to identify the matching pair of parameters (distance between sensors and the crack and size of the crack) the least squares method might be used within these two loops. Since each curve refers to one specific crack length, some curves can be defined as

critical. Therefore, a simple intrinsic damage assessment might follow this step as well. The whole procedure is summarized in Fig. 20.

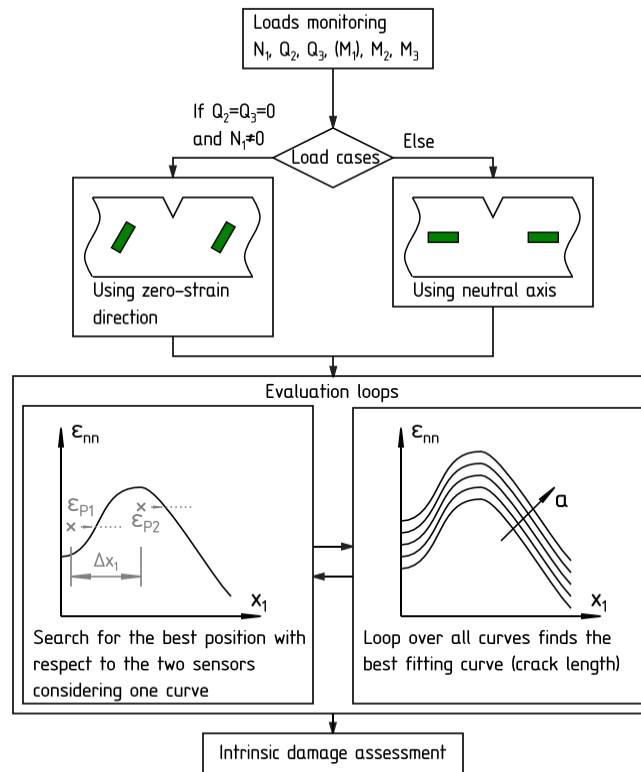


Fig. 20: General procedure using SDIs for generally loaded beam structures

## VI CONCLUSION

This contribution introduced SDIs along with structural analyses as potential key-part of SHM. Structural analyses can be used in order to optimize sensor sensitivity and measurement effort (i.e. the number of sensors). The measurement effort is reduced by focusing on so-called hot spots due to fatigue. Accidental damages were not considered. Structural analyses considering the expected damage were performed in order to identify the change in the structural behavior due to damage. This work suggests focusing on zero baseline damage indicators. As demonstrated in Eq. (2), a reference value of zero (or close to zero), leads to an (almost) infinite relative change, indicating high sensitivity with respect to damage by a simple *True* or *False* statement. Only in case of a damage, a deviation from zero is measured. This SDI can be monitored with common strain sensing technologies (e.g. strain gages or fiber optical sensors). Fig. 11 supports this statement. It shows that relative change in strain close to the crack tip decreases rapidly due to high reference values. On the other hand, there is a high relative change in strain on the neutral axis (as baseline-free sensor location), even at greater distances. In addition, structural models are used in order to provide a digital baseline. Based on the analysis certain threshold values can be defined and used for an efficient intrinsic damage assessment.

In case of beam structures under pure bending, the strain at the nominal neutral axis was presented as a very efficient SDI. Test results showed a clear damage signal in case of a crack. Additional non-linear numerical analyses including plastic material behavior demonstrated that the damage can be detected before residual strength falls below a well-defined design load. We conclude that the damage can be detected before it becomes critical. In case of truss structures under tension, zero-strain directions were derived as a solely material-dependent property. If a crack is present, strain within these specific directions deviates from zero. Numerical studies demonstrated that approach. Damage detection was also successful in this case before the residual strength fell below the design load.

Combining both monitoring approaches for bending beams and truss structures, arbitrary beam structures can be monitored. Such structures are widespread within civil engineering, aerospace engineering and automotive engineering. Many complex structures can be divided into beam elements and shell elements. For example, in a stiffened panel, the stiffener, respectively the super-stiffener (consisting of the stiffener and the adjacent field of the skin) can be considered as beam element. Therefore, the presented approach can easily be transferred to common lightweight constructions without further restrictions.

## ACKNOWLEDGEMENTS

The financial support by the Austrian Federal Ministry of Science, Research and Economy and the National Foundation for Research, Technology and Development is gratefully acknowledged.

## REFERENCES

- [1]. C. Boller, New Trends in Structural Health Monitoring, in *Structural Health Monitoring – Its Association and Use* (Springer, 2013).
- [2]. Handbook Structure Analysis, Industry Committee for Structure Analysis, 2015.
- [3]. CS-25 – Certification Specifications for Large Aeroplanes, European Aviation Safety Agency, 2010.
- [4]. FAR Part 25 – Airworthiness Standards: Transport Category Airplanes, Federal Aviation Administration, 2010.
- [5]. A. Rytter, *Vibration Based Inspection of Civil Engineering Structures*. doctoral diss., Department of Building Technology and Structural Engineering, Aalborg University, Denmark, 1993.
- [6]. C. R. Farrar and K. Worden, An introduction to structural health Monitoring, in *Philosophical Transactions of the Royal Society of London A: Mathematical, Physical and Engineering Sciences 365(1851)*: 303-315, 2017.
- [7]. D. H. Sigurdardottir, *Strain-based monitoring methods for beam-like structures*. doctoral diss., Department of Civil and Environmental Engineering, Princeton University, USA, 2015.
- [8]. R. N. Soman, P. H. Malinowski and W. M. Ostachowicz, Bi-axial neutral axis tracking for damage detection in wind-turbine towers, in *Wind Energy 19(4)*: 639-650, 2015.
- [9]. K.-U. Schröder, A. Preisler, C. Viechtbauer and M. Schagerl, On the Damage Diagnosis based on Structural Analysis Data, in V. Le Cam, L. Mevel and F. Schoefs (eds.), *EWSHM – 7th European Workshop on Structural Health Monitoring*, 2014.
- [10]. A. Preisler, C. Steenbock and K.-U. Schröder, Crack diagnosis of metallic profiles based on structural damage indicators, in *11th International Conference on Damage Assessment of Structures (DAMAS2015)*, *Journal of Physics: conference Series 628*, 2015.
- [11]. K.-U. Schröder, C. Viechtbauer and M. Schagerl, Identification and Monitoring of Structural Parameters as Damage Indicators for Plates in the Post-Buckling Regime, in F.-K. Chang (ed.), *Structural Health Monitoring – A roadmap to Intelligent Structures 2*: 1137-114, 2013.
- [12]. A. Barré de Saint-Venant, Memoire sur la Torsion des Prismes, in *Mem. Dives Savants*, 1853.
- [13]. M. Schagerl, C. Viechtbauer and M. Schaberger, Optimal Placement of Fiber Optical Sensors along Zero-strain Trajectories to Detect Damages in Thin-walled Structures with Highest Sensitivity, in F.-K. Chang (ed), *Structural Health Monitoring 2015 – System Reliability for Verification and Implementation 1*: 1096-1103, 2015.

Andreas Preisler." Intrinsic Damage Assessment of Beam Structures Based On Structural Damage Indicators." American Journal Of Engineering Research (AJER), Vol. 7, No. 6, 2018, Pp.56-70.